

# Kinetics of the Reaction between Sulfur Dioxide and Calcium Oxide at a Low Temperature: Mathematical Modeling

## Cinética de la reacción entre dióxido de azufre y óxido de calcio a baja temperatura: modelado matemático

Isnel Benítez Cortés <sup>1</sup>, Reni Danilo Vinocunga-Pillajo <sup>2</sup>, Luis Beltrán Ramos Sánchez <sup>3</sup>, Agustín García Rodríguez <sup>4</sup>, Estela Guardado Yordi <sup>5</sup>, Gretty Márquez Peñamaría <sup>6</sup>, and Amaury Pérez Martínez <sup>7</sup>

### ABSTRACT

The use of high-sulfur crude oil in power generation plants has increased SO<sub>2</sub> emissions and reduced the service life of steam generators due to corrosive effects in the low-temperature zone, with consequent economic and environmental impacts. The introduction of SO<sub>2</sub> reduction technology using CaO requires an understanding of how the reacting system develops, its governing parameters, the stages controlling the reaction rate, and the kinetic model to which it conforms, among other critical aspects. The objective of this study was to determine the kinetic parameters characterizing the reaction between SO<sub>2</sub> and CaO at low temperatures, as described by the unreacted core model. In a laboratory-scale facility, the reaction temperature was set at 200, 300, and 400 °C, and the SO<sub>2</sub> concentration in air at 2%, 4%, and 6%. Gas-film resistance and gas diffusion within the solid bed were eliminated. The results showed that the rate-controlling step is the resistance of the product layer. SO<sub>2</sub> reduction increased with rising temperature and SO<sub>2</sub> concentration, and CaO conversion did not exceed 20%. The pre-exponential factor was  $2.938 \times 10^{-14}$  m<sup>2</sup>/s, and the activation energy was 17.23 kJ/mol, values characteristic of processes limited by physical diffusion.

**Keywords:** activation, desulfurization, diffusivity, thermogravimetry, unreacted core model

### RESUMEN

El uso de petróleo crudo con alto contenido de azufre en plantas de generación de energía ha incrementado las emisiones de SO<sub>2</sub> y reducido la vida útil del generador de vapor debido a los efectos corrosivos en la zona de bajas temperaturas, con el consecuente impacto económico y medioambiental. La introducción de una tecnología de reducción del SO<sub>2</sub> con CaO requiere comprender cómo se desarrolla el sistema reaccionante, cuáles son sus parámetros, las etapas que controlan la velocidad de reacción y el modelo cinético al que se ajusta, entre otros aspectos de gran importancia. El objetivo de este trabajo fue determinar los parámetros cinéticos que caracterizan la reacción entre el SO<sub>2</sub> y el CaO a bajas temperaturas, descritos por el modelo cinético del núcleo sin reaccionar (NSR). En una instalación a escala de laboratorio se ajustó la temperatura de reacción en los valores de 200, 300 y 400 °C, y la concentración de SO<sub>2</sub> en aire en 2%, 4% y 6%. Se eliminó la resistencia de la película gaseosa y la difusión del gas dentro del lecho de sólidos. Como resultado, la etapa controlante de la velocidad es la resistencia de la capa de producto. La reducción de SO<sub>2</sub> aumenta con el incremento de la temperatura y la concentración de SO<sub>2</sub>, y no se alcanzan valores de conversión del CaO por encima del 20%. El factor preexponencial es  $2,938 \times 10^{-14}$  m<sup>2</sup>/s y la energía de activación es de 17,23 kJ/mol, valores característicos de procesos limitados por difusión física.

**Palabras clave:** activación, desulfuración, difusividad, termogravimetría, modelo de núcleo no reaccionado

**Received:** July 12<sup>th</sup>, 2025

**Accepted:** February 9<sup>th</sup>, 2026

<sup>1</sup> Ph.D., Universidad de Camagüey Ignacio Agramonte Loynaz, Cuba. Chem. Eng., Universidad de Camagüey Ignacio Agramonte Loynaz, Cuba. Full Professor, Universidad de Camagüey Ignacio Agramonte Loynaz, Cuba. Email: isnel.benites@reduc.edu.cu

<sup>2</sup> M.Sc. in Agroindustry, Universidad Estatal Amazónica, Ecuador. B.Eng. in Agroindustrial Engineering, Universidad Estatal Amazónica, Ecuador. Academic Researcher, Universidad Estatal Amazónica, Ecuador. Email: rd.vinocungap@uea.edu.ec

<sup>3</sup> Ph.D., Universidad de Camagüey Ignacio Agramonte Loynaz, Cuba. Chem. Eng., Universidad de Camagüey Ignacio Agramonte Loynaz, Cuba. Full Professor, Universidad de Camagüey Ignacio Agramonte Loynaz, Cuba. Email: luis.ramos@reduc.edu.cu

<sup>4</sup> Ph.D., Technische Universität Dresden (TU Dresden), Germany. Chem. Eng., Universidad Central "Marta Abreu" de Las Villas, Cuba. Full Professor, Universidad Central de Las Villas, Cuba. Email: agarcia@uclv.edu.cu

<sup>5</sup> Ph.D., Universidad de Santiago de Compostela, Spain. B.Sc. in Pharmacy, Universidad de Camagüey, Cuba. Assistant Professor, Universidad Estatal Amazónica, Ecuador. Email: e.guardadoy@uea.edu.ec

<sup>6</sup> M.Sc., Universidad de Camagüey Ignacio Agramonte Loynaz, Cuba. B.Sc. in Chemistry, Universidad de Oriente, Cuba. Full Professor, Universidad de Camagüey Ignacio Agramonte Loynaz, Cuba. Email: greti.marquez@reduc.edu.cu

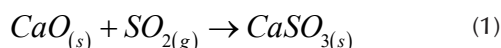
<sup>7</sup> Ph.D., Universidad de Camagüey Ignacio Agramonte Loynaz, Cuba. Chem. Eng., Universidad de Camagüey Ignacio Agramonte Loynaz, Cuba. Associate Professor, Universidad Estatal Amazónica, Ecuador. Email: amperez@uea.edu.ec



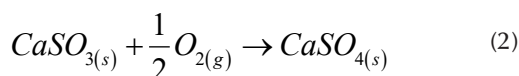
## Introduction

The use of crude oil with a sulfur content exceeding 4% in thermoelectric plants has significant implications for pollutant emissions and desulfurization processes [1], leading to problems such as corrosion in the low temperature zone of the boiler and increased SO<sub>2</sub> emissions into the atmosphere [2].

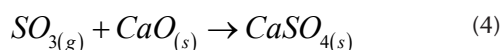
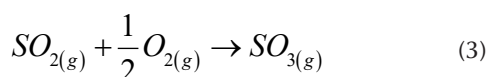
To remove SO<sub>2</sub> from combustion gases, the use of lime, limestone, or lime slurry is well established in the scientific community [3], [4], [5], [6]. In all three cases, the most important reaction is that between lime and sulfur dioxide, as expressed in (1):



At elevated temperatures, oxidation processes continue and the final reaction product is calcium sulfate, as expressed in (2):

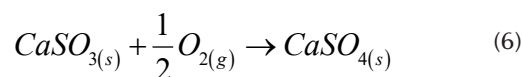
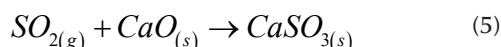


These are recognized as complex reactions due to the high temperatures and short reaction times involved, which reduce diffusion through the pore structure and ash layer [7], [8]. According to (1), when the temperature is below 500 °C, the principal product is CaSO<sub>3</sub>, comprising 32.5% CaO and 46.6% SO<sub>3</sub>, which may also exist in hydrated form. When the temperature exceeds 700 °C, the product obtained is CaSO<sub>4</sub> [9]. Three formation mechanisms have been identified in the literature [10], [11]. The first mechanism occurs in the presence of oxygen, for which CaSO<sub>4</sub> formation is probable, as shown in (3) and (4). The oxidation of SO<sub>2</sub> to SO<sub>3</sub> happens after the reaction between CaO and SO<sub>2</sub>:



The reaction rate given in (3) applies in the absence of a catalyst at temperatures below 1373 °C. In practical combustion processes, SO<sub>3</sub> appears in the gas phase as a result of high-temperature oxidation of SO<sub>2</sub>. It has been reported [12] that the rate of SO<sub>2</sub> removal is independent of O<sub>2</sub> concentration and that SO<sub>3</sub> does not act as an intermediate in the reaction, although its formation may depend on O<sub>2</sub> concentration. Therefore, (3) and (4) do not represent the governing mechanism of CaSO<sub>4</sub> formation [13].

The second mechanism is based on the following equations:



Here, (5) represents the initial step of the desulfurization reaction, and (6) represents the final step. However, because the molar volume of CaSO<sub>4</sub> exceeds that of CaSO<sub>3</sub>, complete pore closure may occur at the external surface of the particles, especially at a low temperature. Under these conditions, CaSO<sub>3</sub> cannot be oxidated to form CaSO<sub>4</sub>, and the reaction is halted. Moreover, it has been confirmed that CaSO<sub>4</sub> is one of the products of the reaction between CaO and SO<sub>2</sub> [14] within the temperature range of 200–600 °C.

An increase in temperature above this range enhances effective diffusivity. Consequently, the product layer of the sulfate particle develops more open pores, which facilitates the formation of CaSO<sub>4</sub>.

Experiments conducted at low temperatures, such as 300 °C, in the presence and absence of oxygen, showed that the compound formed was CaSO<sub>3</sub> [9]. It has also been reported that the adsorption mechanism of SO<sub>2</sub> on CaO is not well established in the specialist literature. At low temperatures, the kinetic treatment proceeds according to (1).

Although the reaction of lime with SO<sub>2</sub> has been widely investigated, no kinetic study using Cuban lime has been reported in the literature. This study therefore addresses a gap by characterizing the reaction system between SO<sub>2</sub> and Cuban lime. Several models have been proposed to describe the reaction under study; for instance, the model developed in [16] simultaneously analyzes calcination, sintering, and sulfation, in which sorbent decomposition follows the unreacted core model (UCM). However, the majority of existing models focus on large particle sizes, long contact times, and temperatures exceeding 850 °C. The UCM has also been applied in [17], [18], and [19].

Several researchers have treated the sulfation reaction as first-order with respect to both SO<sub>2</sub> and CaO, reporting rate constants in the range of 0.001 to 0.02 m<sup>3</sup>/mol [20]. Applying the UCM, [17] reported a rate constant of 0.05–0.5 m/s, while [21] obtained a diffusion coefficient of 2 × 10<sup>-11</sup> m<sup>2</sup>/s. The apparent activation energy reported in [22] span a notably wide range, from 6.64 to 82.18 kJ/mol for five limestones. Meanwhile, activation energies of 100.9 ± 2.2 kJ/mol for pure limestones, 115.6 ± 3.5 kJ/mol for dolomites, and 84.1 ± 0.4 kJ/mol for marly limestones were reported in [23].

A UCM was developed in [21] to describe the mechanism of the non-catalytic reaction between CaO and SO<sub>2</sub>, demonstrating good correlation between the model and the diffusion-controlled behavior, with the ash layer identified as the rate-limiting step. Independent of the model used to characterize the reactant system for SO<sub>2</sub> and CaO, the activation energy was around 104.5 to 171.38 kJ/mol (25–41 kcal/mol), while the effective diffusivity ranged from 0.19 to 0.428e<sup>-12</sup> m<sup>2</sup>/s, both determined at elevated temperatures

(800–1.000 °C). These results indicated that the UCM is the most commonly applied model for kinetic analysis of this system.

Accordingly, this study proposes the determination of kinetic parameters, including the pre-exponential factor, activation energy, and conversion, together with the kinetic model that describes the reaction in the 200–400 °C range, where corrosion occurs due to the sulfuric acid formation and which has not been previously documented in the literature. These findings are expected to contribute to the development of technology aimed at reducing SO<sub>2</sub> in combustion gases, thereby mitigating both corrosive effects and environmental impact.

The manuscript is structured as follows. The Methods section presents the methodological flowchart and the procedure followed to validate the research hypothesis. The morphological characterization of CaO particles is described, along with the design and assembly of the experimental setup and the operational techniques applied during testing. The procedures implemented to minimize gas-phase resistance and gas diffusion between particles are detailed, with the objective of determining the intrinsic reaction rate. The experimental design, the criteria used for fitting the UCM, and the corresponding procedure are also presented. Finally, the results obtained are reported and discussed.

## Methods

### Flowchart of the methodological phases

Fig. 1 presents the methodological structure of the study, divided into five sequential phases: the physicochemical characterization of CaO, the installation of the experimental system, factorial experimentation under controlled conditions, determination of conversion through gravimetric analysis, and the mathematical modeling based on the UCM. Each stage was designed to ensure experimental reproducibility and reliable kinetic interpretation of the CaO–SO<sub>2</sub> reaction.

The characterization process included the chemical composition of lime and its particle size distribution.

### Chemical composition

The chemical composition of lime was determined at the central laboratory of the Geominera Company, Camagüey, according to the ASTM C25, Standard Test Methods for Chemical Analysis of Limestone, Quicklime, and Hydrated Lime.

### Particle size distribution

Particle size distribution was determined by sieving analysis performed in the Unit Operations Laboratory of the University of Camagüey Ignacio Agramonte Loynaz. WLW-RDA vibratory sieving equipment (RDA) was used for this purpose. Eight clean sieves ranging from -12+16 to -400 mesh were stacked in descending order of aperture size. Wet sieving was performed using water as the sieving medium, given the small particle size, and continued until the effluent ran clear. Solid samples were dried in a Memmert oven at 100 °C, and 200 g of the sorbent was weighed for each test. The samples were then sieved twice, and the average values were recorded. After the samples were dried in the oven, the retained fractions were weighed using an analytical balance with a precision of 0.001 g.

A preliminary visual inspection of Cuban lime indicated that the majority of particles are very small, without undergoing any physical size reduction. Further characterization of these particles is therefore recommended, as detailed below. Moreover, the following parameters are needed to use the kinetic model of the unreacted nucleus:

### Particle size distribution for small particles

A total of 1.098 particles with diameters below 40 µm (see Results of the screening analysis section) were analyzed using a Hitachi S-4100 scanning electron microscope, equipped with a BSE AuTrata detector, an EMIP 3.0 image capture system, and a Röntec microanalysis system. The length and width of each particle were measured, the area was determined by assuming a rectangular cross-sectional shape, and the equation for the area of a circle was applied to obtain the equivalent diameters and corresponding radius.

### Approximation to the shape of particles

The shape of the particles is one of the most critical aspects for fitting the unreacted nucleus model, as the appropriate model formulation depends on whether the particles are cylindrical, flat, or spherical. For instance, micrographs of the particles were taken using the scanning electron microscope.

### Weight loss associated with the evaporation of water and release of volatile compounds

Kinetic studies for this type of reaction system are performed using the gravimetric method. Therefore, it is necessary to ensure that the weight variations experienced by the sorbent are caused by physical processes such as drying, loss of volatile substances, or moisture absorption, factors unrelated

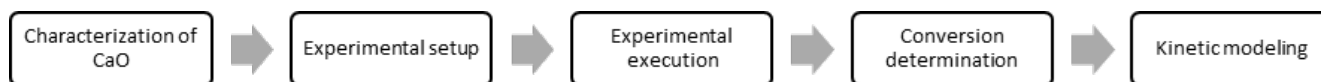


**Figure 1.** Flowchart of the experimental methodology applied in the kinetic modeling of the CaO–SO<sub>2</sub> reaction

Source: Authors



°C, with an SO<sub>2</sub> concentration of 6% and a rotational speed of 1 rpm. The gas flow rate was varied within the range of 0.103 to 0.172 NL/s. The objective was to identify the minimum flow rate at which the mass transfer limitations in the gas phase could be considered negligible.

The gas mixture was prepared using calibrated flowmeters, and the SO<sub>2</sub> concentration was held constant throughout the experiment. The weight gain of the lime sample was recorded every 10 minutes using a Sartorius analytical balance. The data obtained were plotted to assess the effect of gas flow on the conversion of CaO to CaSO<sub>3</sub>.

### Minimum rotational speed of the reactor

The objective of this experiment was to determine the minimum rotating speed of the reactor necessary to eliminate gas diffusion resistance among particles. The experimental setup was maintained under the same operational conditions as the gas flow test, at a constant temperature of 400 °C and SO<sub>2</sub> concentration of 6%.

The rotational speed was systematically varied in the range of 0 to 0.75 rpm to assess its effect on gas diffusion and particle interaction. The weight gain of the lime sample was recorded every 10 minutes using a Sartorius analytical balance. The recorded data were plotted to evaluate the effect of rotational speed on the conversion of CaO to CaSO<sub>3</sub>.

### Experimental design

To evaluate the influence of SO<sub>2</sub> concentration and temperature on the reaction rate, a factorial design of type 3<sup>3</sup> was applied. The experimental conditions included SO<sub>2</sub> concentrations of 2, 4, and 6% in air, combined with temperatures of 200, 300, and 400 °C. These combinations allowed for an analysis of the reaction kinetics under varying operational parameters.

The experimental procedure involved recording the weight gain over time for each combination of SO<sub>2</sub> concentration and temperature. The data were processed using a fifth-order polynomial regression analysis with Statgraphics Plus v. 5.0. This approach enabled the estimation of conversion values and facilitated the identification of trends in the reaction rate based on the defined variables.

### Sulfation reaction modeling

The UCM was selected to describe the reaction kinetics of SO<sub>2</sub> with lime particles under the defined experimental conditions. This model is widely utilized to characterize gas-solid reactions involving porous particles, particularly under conditions where both diffusion resistance and surface reaction are considered. Table 1 presents the key assumptions and considerations applied in the development of the UCM for this study.

**Table 1.** Assumptions and hypotheses for the application of the unreacted core model (UCM) in the sulfation reaction of lime.

Hypothesis	Description
Reaction pathway	The sole reaction considered is the sulfation of lime to calcium sulfite, as described in (5).
Model adjustment	Experimental data are assumed to align with the UCM, considering a constant effective diffusivity.
Temperature profile	Temperature gradients within particles are negligible, allowing for an isothermal treatment.
State of products	All products remain in a solid state. The ash layer does not form a barrier or hinder the reaction.
Reaction site	The reaction occurs exclusively at the surface of the unreacted core, consistent with UCM principles.
SO <sub>2</sub> concentration	The concentration of SO <sub>2</sub> in the gas phase and at the particle surface remains constant throughout the process.
Gas flow rate	Gas flow rates are sufficiently high to eliminate mass transfer resistance in the gas phase.
Particle state	Solid particles are maintained in a turbulent state, allowing the neglect of interparticle mass transfer resistance.
Controlling steps	The model considers resistance to diffusion through the product layer and the surface reaction as the only controlling steps.
Pseudo-steady state	The reaction is treated under pseudo-steady-state conditions due to the slow surface reaction relative to SO <sub>2</sub> diffusion.

Source: Authors.

### Description of the algorithm of adjustments

Various authors [25], [26] have demonstrated that solid-gas reactions involve a series of factors to be taken into account in the kinetic model, including the presence of a solid size distribution, the variation in their form, and the difference in reactivity between the components. Previous researchers have proposed dividing the solids into “n” groups according to the particle size and computing an average conversion based on the particle size distribution ( $f_{(R_i)}$ ), the conversion of isolated particles ( $X_{(t,v)}$ ), and the particle radius ( $R_i$ ), as expressed in (8):

$$\bar{X}_{(R)} = \int_{Rmin}^R f_{(R_i)} dR + \int_R^{Rmax} f_{(R_i)} X_{(\hat{o},t)} dR \quad (8)$$

The first term considers the particles that have been totally converted, and the second considers the particles that have not been totally converted. The procedure for obtaining the conversion is as follows:

1. The calculation begins with fixed system parameters, such as lime molar density (69.56 mol/m<sup>3</sup>), the stoichiometric coefficient (b=1), and the reaction order (n=1).
2. For each particle radius level ( $R_{min}$  to  $R_{max}$ ), temperature, partial pressures, and time (t) at which the average conversion is evaluated, the conversion is estimated by

the numerical integration of (8), where  $f_{(R)}$  is obtained using (15).

3. The conversion in the isolated particle is obtained by numerical solution of (9), using the Newton-Raphson method:

$$t = 3\tau_{CZ} \left[ Z - \frac{Z - \left( (1-Z)(1-X)^{\frac{2}{3}} \right)}{(Z-1)} - (1-X)^{\frac{2}{3}} \right] + \tau_{RQ} \left[ 1 - (1-X)^{\frac{1}{3}} \right] \quad (9)$$

This expression corresponds to the UCM kinetic model with constant effective diffusivity. The term  $Z$  represents the molar volume ratio, which must be included in the equation when modeling reactions with significant differences between molar volumes of the reactant and the product [19]. Specifically,  $Z$  corresponds to the ratio of molar volumes of the product formed and the reactant ( $\text{CaSO}_3/\text{CaO}$ ). The molar masses of  $\text{CaSO}_3$  and  $\text{CaO}$  are 120.14 g/mol and 56.08 g/mol, respectively, while their densities are 2.5–2.6 g/cm<sup>3</sup> and 3.34 g/cm<sup>3</sup>, yielding molar volumes of 47 cm<sup>3</sup>/mol and 16.8 cm<sup>3</sup>/mol, respectively. These values result in  $Z = 2.79$ . This value can change depending on the temperature and pressure at which the reaction takes place. In the UCM modeling process, this parameter is considered in the simulation to evaluate its behavior for Cuban lime at low temperatures. The simulation begins with a value of 1.247 [27].

The remaining terms in (9) are calculated as follows:

$$\tau_{RQ} = \frac{\rho_s}{bk_s C(\text{SO}_2)} R \quad (10)$$

$$\tau_{CZ} = \frac{\rho_s}{6bD_e C(\text{SO}_2)} R^2 \quad (11)$$

where:

$$k_s = A_{RQ} e^{\left[ \frac{E_{RQ}}{RT} \right]} \quad (12)$$

$$D_e = B_{CZ} e^{\left[ \frac{E_{CZ}}{RT} \right]} \quad (13)$$

4. Initial values of pre-exponential factors ( $A$  and  $B$ ) and the activation energies ( $E_{RQ}$  and  $E_{CZ}$ ) were taken from values reported in the literature to define the first dataset.
5. The objective function to adjust is expressed in (14):

$$\text{MIN : FO} = \frac{\sum_1^Z \sum_1^N \left( \frac{\bar{X}_{cal}}{\bar{X}_{exp}} - 1 \right)^2}{E_{EXP}} \quad (14)$$

If the calculated error is not acceptable, the values of  $A$ ,  $B$ ,  $E_{RQ}$  and  $E_{CZ}$  are changed following the numerical optimization method until the error becomes minimal. The Hooke and Jeeves method [28] was employed for this purpose, and the algorithm was implemented in Visual Basic v. 5.0.

## Results and discussion

### Chemical composition of Cuban lime

The chemical composition of the sorbent confirms its high CaO content, which is favorable for its application in flue gas desulfurization technologies. The presence in very low concentrations of magnesium oxides, aluminum, iron, and silicon leads us to consider that, in the kinetic study, CaO is solely responsible for the reduction of sulfur dioxide, as shown in Table 2.

**Table 2.** Chemical composition of Cuban lime

CaO	MgO	SiO <sub>2</sub>	Al <sub>2</sub> O <sub>3</sub>	Fe <sub>2</sub> O <sub>3</sub>	Ignition losses
64.80	0.21	3.15	2.07	0.25	29.67

**Source:** Authors.

The chemical composition analysis confirmed a CaO purity exceeding 90%, which indicates a sorbent highly suitable for SO<sub>2</sub> capture. The low concentrations of residual oxides imply that CaO acts as the main reactive phase, consistent with the results reported in [29] and [30]. This high purity also supports the application of reliable kinetic models. In this regard, it has been shown that well-characterized materials with minimal interference from inert phases allow more accurate prediction in heterogeneous systems, even in complex media such as crude-solvent emulsions [31]. Therefore, the high purity of the CaO used in this study reinforces its suitability for modeling diffusion-governed reactions [32].

### Particle size distribution

Table 3 presents the results of the sieving test. For a total initial sample mass of 200 g, 91.5% passed through the 40 μm sieve. This result is significant because it indicates that the material is suitable for kinetic studies, which require small particle sizes to minimize diffusion resistance in the product layer.

**Table 3.** Results of the screening analysis.

Mesh class	Retained mass (g)	Fraction	Particle diameter (mm)	Cumulative Retained Fraction	Average (mm)	Non-accumulated fraction
-12+16	1.18	0.0059	1.397	0.006	1.194	0.994
-16+28	0.44	0.0022	0.991	0.008	0.790	0.992

-28 +35	0.28	0.0014	0.589	0.010	0.503	0.991
-35 +115	0.81	0.0040	0.417	0.014	0.270	0.987
-115+200	1.59	0.0080	0.124	0.022	0.114	0.979
-200 +350	5.18	0.0259	0.104	0.047	0.089	0.953
-350 +400	7.36	0.0368	0.074	0.084	0.056	0.916
-400	183.46	0.9173	0.038	0.998	—	0.002

Source: Authors.

### Particle size distribution for small particles

Particle radius values ranged from 0.874 to 37.490 μm. These data were fitted to an empirical power-type distribution, with the mean of 8.5808 μm and the standard deviation of 7.888 μm, yielding a coefficient of determination of R<sup>2</sup> = 0.8855. The particle size distribution was fitted to an empirical model expressed in (15):

$$f_{(R_i)} = 5,0928 \times 10^{-10} R^{-1,6827} \quad (15)$$

where R is the diameter of the Cuban lime particles in μm (Fig. 3).

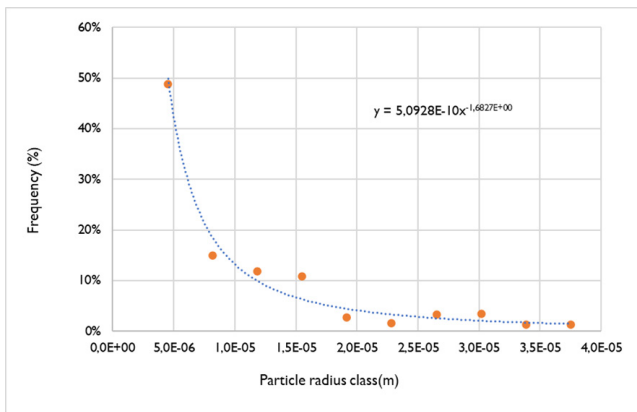


Figure 3. Frequency distribution of particle radius for Cuban lime particles.

Source: Authors.

### Approximation of particle shape

Fig. 4 presents the particle shape characterization results. The analysis indicates that the shape of the particles tends toward a spheroidal geometry; this approximation was therefore adopted for use in kinetic modeling.

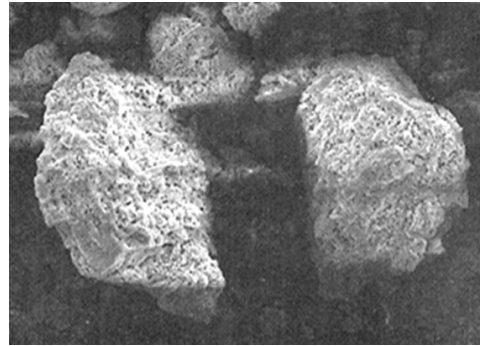


Figure 4. Microelectronic photograph of the sorbent (enlargement 1 mm: 1 000 nm).

Source: Authors.

### Weight loss associated with the evaporation of water and release of volatile compounds

For the uncalcined absorbent, a considerable weight loss due to evaporation was observed, indicating that thermal pretreatment is required prior to use as a reactant in order to eliminate both moisture and volatile compounds.

TGA confirmed a significant mass loss during the heat treatment at 580 °C, attributable to the elimination of water and volatile compounds. The stabilization step at 110 °C prevented rehydration, maintaining the consistency of the samples. It was observed that more than 92 % of the particles had diameters of less than 40 μm. The empirical model reached an R<sup>2</sup> of 0.8855, with a standard deviation of 7.888 μm and a mean diameter of 8.5808 μm. These three results are comparable to those reported in [33], which also demonstrated that thermally stable structures improve the reliability of predictive model applications. The study indicates that the pre-treatment must be carried out at a minimum temperature of 580 °C, primarily because calcium hydroxide, which is invariably present in a CaO samples exposed to atmospheric air, decomposes at this temperature. Therefore, all sorbent samples were subjected to a 24-hour pre-treatment at 580 °C to eliminate all volatile substances (Table 4).

Table 4. TGA results.

Uncalcined sorbent				
No.	Δ T. (°C)	Weight loss (%)	T(°C)*	Origin
1	25–110	0.8	72	Loss of moisture and absorbed water
2	110–300	1.19	182	Decomposition of hydroxides
3	300–500	14.91	442	
4	500–800	14.02	711	Decomposition of carbonates

5	800–1200	0.23	855	Loss of volatiles
Total	110–1200	30.4		
Sorbent calcined at 580°C.				
No.	$\Delta T$ . (°C)	Weight loss (%)	T(°C)*	Origin
1	25–110	-0.41	78	Weight gain: Hydration, oxidation, and carbonation
2	110–300	-1.52	186	
3	300–500	5.75	394	Decomposition of hydroxides
4	500–800	12.7	711	Decomposition of carbonates
5	800–1200	0.21	920	Loss of volatiles
Total	110–1200	17.2		

\* Temperature at which the rate of weight loss is at its maximum.

Source: Authors.

### Specific surface area

The morphological analysis of Cuban lime evidenced that calcination increased pore diameters from 23.4–27.4 nm (uncalcined) to 30.6–33.1 nm (calcined). Despite this increase, the specific surface area remained in a stable range of 13 to 13.3 m<sup>2</sup>/g, indicating that the porosity was not significantly affected by the heat treatment. These results coincide with observations reported in [31], which noted that surface area stability is a critical factor to guarantee efficiency in mass transfer processes, especially in predictive models based on porous structures. Consequently, the preservation of the microstructure of the calcined CaO in this study supports its viability for diffusion-governed applications without compromising its reactive capacity.

A significant difference was observed between the pore diameter of the sorbent without prior treatment and with prior treatment. These results indicate that thermal pre-treatment of the solid surface widens the pores by approximately 20–30%, slightly increasing its absorption capacity. The increase in pore size is associated with the loss of organic and volatile material, which, upon removal, increases the cross-sectional area of the pores where it is located. An additional contributing factor is the decomposition of the calcium hydroxide present in the material at temperatures above 580 °C, which modifies the particle structure and induces particles cracking, further increasing pore size. As shown in Table 5, the specific surface area does not vary considerably between the calcined and uncalcined sorbent.

Table 5. Specific surface area

Additive	Average diameter in adsorption (nm)	Average diameter during desorption (nm)	Specific surface area (m <sup>2</sup> /g)
Uncalcined sorbent	27.4	23.6	13.0
Sorbent calcined at 580°C.	33.1	30.6	13.3

Source: Authors.

### Effect of gas flow rate on reaction rate

Experimental results show that for flow rates below 0.117 L/s, notable differences in mass gain are observed (Fig. 5), suggesting that the diffusion of SO<sub>2</sub> in the gas phase limits the conversion of CaO. In contrast, at flow rates of 0.127, 0.151, and 0.172 L/s, the weight gain curves overlap, confirming that the mass transfer resistance has been overcome and that the reaction rate is determined by the intrinsic kinetics of the gas-solid system. This behavior was consistent across the three temperature levels investigated, with mass gain increasing with temperature. These findings are consistent with those reported in [9], which indicated that under similar conditions, the CaO-SO<sub>2</sub> reaction transitions from a diffusion-controlled regime to one governed by chemical kinetics. Accordingly, a flow rate of 0.172 L/s was selected for the subsequent experiments, ensuring that the mass transfer resistance did not limit the reaction rate.

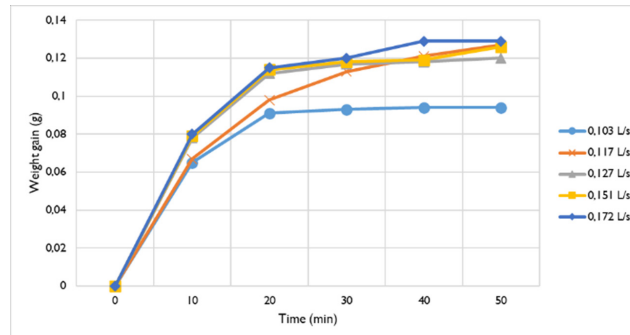


Figure 5. Effect of gas flow on the conversion of lime.

Source: Authors.

### Effect of rotational speed on reaction rate

At rotational speeds below 0.75 rpm, the weight gain curves show significant differences, evidencing that the diffusion of SO<sub>2</sub> between particles limits the conversion. At static conditions (0 rpm), the gas-solid contact proved insufficient, significantly reducing the diffusion of the reagent. Although moderate mass increases were recorded at 0.25 and 0.5 rpm (Fig. 6), diffusional limitations persisted. At 0.75 rpm, the curves stabilized, signaling a substantial improvement in phase-phase contact. This result is consistent with findings reported in [34] and [35], which demonstrated that rotational agitation favors mass transfer in gas-solid systems. However, internal diffusion through the product layer remains a potential barrier; in materials with irregular morphology, this layer may hinder gas penetration. This

phenomenon has been described in studies of non-catalytic reactions using random pore models [36].

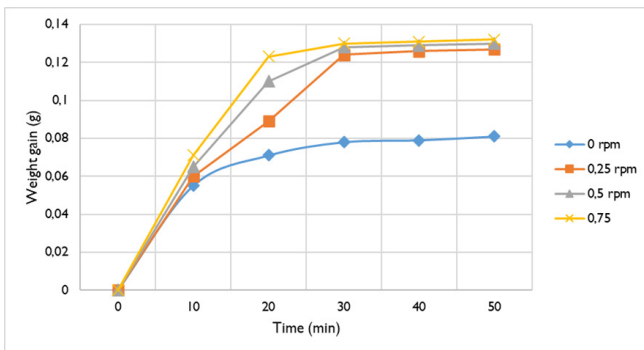


**Figure 6.** Effect of the reactor rotational speed on CaO conversion. **Source:** Authors.

Based on these findings, a rotational speed of 0.75 rpm was selected for subsequent experiments. The stabilization of the weight increment curve at this speed confirms that the reaction rate is primarily controlled by the intrinsic kinetics under these conditions. Nevertheless, the effect of higher rotational speeds should be evaluated in future studies to determine whether further reductions in diffusion resistance can be achieved, especially in cases where the particle size is reduced to less than 10  $\mu\text{m}$ . Such investigations could provide valuable insights into optimizing operational conditions in large-scale applications, such as rotary reactors in industrial desulfurization processes.

### Effect of temperature and $\text{SO}_2$ concentration

The experimental data showed that the conversion levels did not exceed 30–40% under the conditions evaluated, which contrasts with results reported in [37] and [38], where conversions above 60% were recorded at temperatures above 900  $^\circ\text{C}$ . This difference is attributed to the diffusive resistance of the formed product layer, which limited the penetration of  $\text{SO}_2$  and, consequently, the reaction rate. The application of a polynomial regression model enabled more precise quantification of the conversion achieved in the presence of temperature and concentration variations. Despite the thermal increase, the structural barrier imposed by the product layer prevented higher conversion, especially at low  $\text{SO}_2$  concentration conditions. This reinforces the importance of porosity in the efficiency of the process, as established in kinetic studies of non-catalytic reactions with diffusion-limiting mechanisms.

### Comparison between diffusion and chemical reaction

The results presented in Fig. 7 show that the conversion time by chemical reaction is considerably less than that associated with diffusion through the production layer, confirming that diffusional resistance represents the limiting stage in the lime sulfation process. This behavior justifies the omission of the kinetic resistance in the model fit, as expressed in (10). The diffusivity of  $\text{SO}_2$  in layers formed during CaO sulfation has been evaluated in [39], which found that the reduction of the

pore diameter increases this resistance, favoring a diffusion-controlled regime. This coincidence supports the validity of the proposed model, even for particles smaller than 10  $\mu\text{m}$ , in which a dense layer forms and restricts the penetration of the reactive gas.

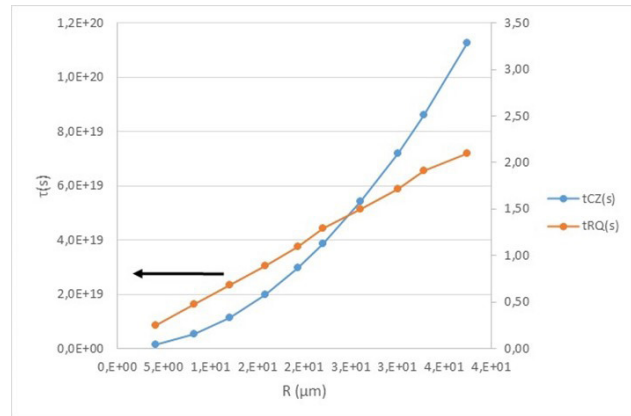


**Figure 7.** Comparison between  $\tau_{\text{RQ}}$  and  $\tau_{\text{CZ}}$  values obtained in the adjustment. **Source:** Authors.

### Adjustment of the UCM model to experimental data

Fig. 8 presents the results of the UCM adjustment to the experimental data obtained at 200, 300, and 400  $^\circ\text{C}$ . The solid lines represent the values calculated by the model, while the circles reflect the empirical data: the green line for 2%  $\text{SO}_2$ , the light blue line for 4%, and the orange line for 6%. At 300  $^\circ\text{C}$ , the conversion exhibited a tendency to stabilize, indicating that the progressive formation of the product layer limits gas penetration, acting as a diffusive barrier. This behavior agrees with findings reported in [4], where diffusional resistance through the solid layer was identified as the determining factor in the control stage of *in situ* desulfurization processes. Despite the adequate correspondence between experimental and calculated values, it is advisable to extend the settings to temperatures above 400  $^\circ\text{C}$  to confirm a possible transition to a fully diffusion-controlled regime.

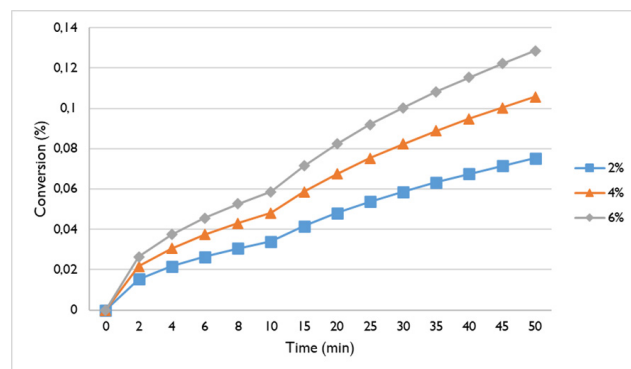


**Figure 8.** Adjustment of the UCM to the experimental results at 300  $^\circ\text{C}$ , in which  $B$  and  $E_{\text{CZ}}$  are reported in Table 1. Solid lines represent the calculated values, and the marked lines represent the experimental data. Similar results have been obtained for 200 and 400  $^\circ\text{C}$ . **Source:** Authors.

The kinetic parameters determined through the adjustment of the UCM model are presented in Table 6. The values obtained for B and  $E_{CZ}$  correspond to a diffusion-controlled process. The activation energy of 17.23 kJ/mol indicates a low temperature dependency. The relative fitting error of 8.09%, demonstrates acceptable correspondence between the experimental data and the values calculated by the model.

**Table 6.** Kinetic parameters obtained by adjusting the UCM.

Parameter	Unit	Value
B	m <sup>2</sup> /s	2.9381x10 <sup>-14</sup>
ECZ	kJ/mol	17.23
Error of adjustment	%	8.09%

**Source:** Authors.

### Evaluation of diffusivity and its relationship with temperature

The experiments were conducted over a temperature range of 200 to 400 °C. The dashed line in Fig. 9 represents the linear trend obtained within this measurement range, with a coefficient of determination of  $R^2 = 0.986$ . As the temperature increased from 200 to 400 °C, the effective diffusivity (ED) values increased, reaching a maximum of  $1.2 \times 10^{-15}$  m<sup>2</sup>/s at 400 °C. Throughout this range, the values remained relatively low, indicating the restriction to SO<sub>2</sub> diffusion due to the formation of a dense product layer. This trend aligns with the activation energy of 17.23 kJ/mol, characteristic of diffusion-controlled processes with low temperature dependence. This behavior is consistent with results reported in [22], which describe the influence of diffusion resistance in the product layer on reaction efficiency during limestone sulfation. The Z value obtained is 1.75, which is higher than the value reported in [27].

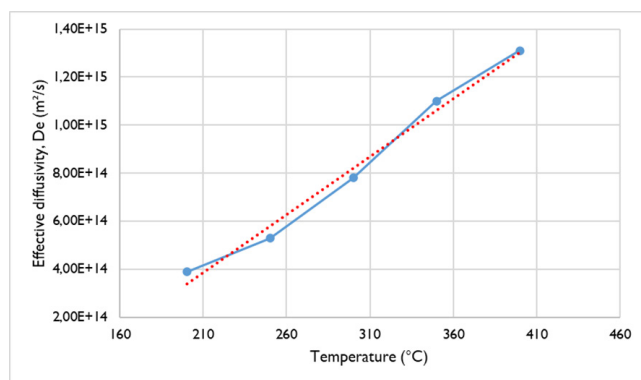


**Figure 9.** Effective diffusivity ( $D_e$ ) of SO<sub>2</sub> in the lime particles, estimated using (13).

**Source:** Authors.

## Conclusions

The results confirm the hypothesis proposed in this study. The chemical reaction between SO<sub>2</sub> and CaO contained in Cuban lime fits the unreacted core model, with effective diffusivity values ranging from  $3.90 \times 10^{-14}$  to  $1.31 \times 10^{-15}$  m<sup>2</sup>/s,

reaching a maximum of  $2.00 \times 10^{-15}$  m<sup>2</sup>/s at 400 °C. Fitting the model to the experimental data yielded a relative error of 8.09%, indicating satisfactory agreement between calculated and measured values. Diffusion through the product layer (CaSO<sub>4</sub>) constituted the main resistance in the process, limiting overall conversion in the 200–400 °C range. The activation energy of 17.23 kJ/mol showed low temperature dependence in diffusion, characteristic of diffusion-controlled processes. These findings are relevant for the design of technologies aimed at SO<sub>2</sub> reduction. The primary limitation identified was the low conversion achieved under the evaluated SO<sub>2</sub> concentrations and temperatures, suggesting the need for future research on the pre-treatment of CaO particle surfaces to increase pore size, as well as the assessment of alternative contact systems with higher efficiency.

## Nomenclature

- $A_{RQ}$  - Frequency factor for the chemical reaction (m/s).
- b - Stoichiometric coefficient (mol of B consumed/mol A reacted)
- $B_{CZ}$  - Frequency factor for diffusion through the ash layer (m<sup>2</sup>/s).
- $D_e$  - Effective diffusivity (m<sup>2</sup>/s).
- $E_{CZ}$  - Activation energy for the diffusion stage through the ash layer (kJ/mol).
- $E_{EXP}$  - Experimental error (%).
- $E_{RQ}$  - Activation energy for the chemical step (kJ/mol).
- $f_{(Ri)}$  - Weight fraction of the different particle sizes in the sample (%).
- $k_s$  - Intrinsic kinetic constant of the reaction rate (m/s).
- R - Initial radius of the particle (m).
- $r_c$  - Radius of the unreacted core (m).
- $r_{ci}$  - Unreacted core radius of particle size i (m).
- $R_i$  - Initial radius of particle size i (m).
- $R_{max}$  - Maximum particle radius (m).
- $R_{min}$  - Minimum particle radius (m).
- t - time (s).
- TGA – Thermogravimetric analysis.
- RDA – WLW-RDA vibratory sieving equipment used for particle size classification.
- UCM: unreacted core model.
- $W_{CaO}$  - Mass fraction of CaO in the sample.
- $W_o$  - Initial weight of the dry sample (g).
- $W_t$  - Increased weight of the sample over time (g).
- $X_B$  - CaO conversion (g CaO converted/g initial CaO).
- $X_{CAL}$  - Calculated conversion (%).
- $X(R)$  - Average conversion of the fraction of size R (mol CaO/mol solid).
- $X_{EXP}$  - Experimental conversion (%).
- $X_{(t,T)}$  - Conversion of the isolated particle according to Eq. (8) (fraction).
- $x_{CaO}$  - CaO content in the sample (%).
- $\tau_{CZ}$  - Time required for the particle to react completely according to the resistance of the physical stage (min).
- $\tau_{RQ}$  - Time required for the particle to react completely according to the resistance of the chemical step (min).
- $\rho_s$  - Apparent mass density of the solid particle (kg/m<sup>3</sup>).

## CRedit author statement

Isnel Benítez Cortés and Luis Beltrán Ramos Sánchez: conceptualization and background review. Amaury Pérez Martínez, Isnel Benítez Cortés, and Estela Guardado Yordi: data collection, workflow developed, and formal analysis. Agustín García Rodríguez and Grety Márquez Peñararúa: supervision and critical review. Reni Danilo Vinocunga-Pillajo and Isnel Benítez Cortés: writing – original draft preparation. All authors: writing – review and editing.

## Conflicts of interest

The authors declare no known competing financial interests or personal relationships that could have influenced the work reported in this article.

## Data availability

The datasets generated and/or analyzed during this study are available from the corresponding author upon reasonable request.

## Acknowledgment

The authors wish to thank Helen Pugh for proofreading the article.

## Statement on artificial intelligence

The authors confirm that no generative Artificial Intelligence (AI) tools were used in the writing, data analysis, or preparation of this manuscript. The authors take full responsibility for the originality and content of the publication.

## References

- [1] A. Demirbas, A. H. Alidrisi, and M. A. Balubaid, "API Gravity, Sulfur Content, and Desulfurization of Crude Oil," *Petroleum Sci. Technol.*, vol. 33, no. 1, pp. 93–101, Jan. 2015. <https://doi.org/10.1080/10916466.2014.950383>
- [2] M. Xu, S. Xue, F. Hu, Z. Jiang, L. Zheng, Y. Ren, Z. Li, S. He, and R. Deng, "Failure case study on reheater pipes in a subcritical unit served for a thermal power plant," *Case Stud. Therm. Eng.*, vol. 59, art. 104550, Jul. 2024. <https://doi.org/10.1016/j.csite.2024.104550>
- [3] N. H. Koralegedara, P. X. Pinto, D. D. Dionysiou, and S. R. Al-Abed, "Recent advances in flue gas desulfurization gypsum processes and applications – A review," *J. Environ. Manage.*, vol. 251, art. 109572, Dec. 2019. <https://doi.org/10.1016/j.jenvman.2019.109572>
- [4] E. S. Go, J. L. J. Ling, B. S. Solanki, H. Ahn, P. L. Show, and S. H. Lee, "Current advances and future prospects of in-situ desulfurization processes in oxy-fuel combustion reactors," *Environ. Res.*, vol. 263, art. 119982, Dec. 2024. <https://doi.org/10.1016/j.envres.2024.119982>
- [5] S. De Gisi, A. Molino, and M. Notarnicola, "Enhancing the recovery of gypsum in limestone-based wet flue gas desulfurization with high energy ball milling process: A feasibility study," *Process Saf. Environ. Prot.*, vol. 109, pp. 117–129, Jul. 2017. <https://doi.org/10.1016/j.psep.2017.03.033>
- [6] L. Koech, R. C. Everson, B. Hattingh, H. Rutto, L. Lerotoli, and H. W. J. P. Neomagus, "Comparative study of sorbents for spray dry scrubbing of SO<sub>2</sub> from flue gases," *ACS Omega*, vol. 8, no. 26, pp. 23401–23411, Jul. 2023. <https://doi.org/10.1021/acsomega.3c00064>
- [7] Y. Huang, Y. Li, M. Zhang, B. Deng, H. Kong, J. Wang, J. Lyu, H. Yang, and L. Wang, "Effective diffusivity of oxygen in the ash layer of Huadian oil shale semicoke," *Front. Energy*, vol. 15, no. 2, pp. 320–327, Jun. 2021. <https://doi.org/10.1007/s11708-020-0674-3>
- [8] D. Liang, Q. Xie, J. Liu, F. Xie, D. Liu, and C. Wan, "Mechanism of the evolution of pore structure during the preparation of activated carbon from Zhundong high-alkali coal based on gas–solid diffusion and activation reactions," *RSC Adv.*, vol. 10, no. 55, pp. 33566–33575, Sep. 2020. <https://doi.org/10.1039/D0RA06105K>
- [9] M. H. Rasmussen, S. Wedel, K. H. Pedersen, J. B. Illerup, and K. Dam-Johansen, "Initial reaction between CaO and SO<sub>2</sub> under carbonating and non-carbonating conditions," *Chem. Eng. Sci.*, vol. 134, pp. 169–177, Sep. 2015. <https://doi.org/10.1016/j.ces.2015.04.051>
- [10] R. Tritippayanon, R. Piemjaiswang, P. Piumsomboon, and B. Chalermisinsuwan, "Computational fluid dynamics of sulfur dioxide and carbon dioxide capture using mixed feeding of calcium carbonate/calcium oxide in an industrial scale circulating fluidized bed boiler," *Appl. Energy*, vol. 250, pp. 493–502, Sep. 2019. <https://doi.org/10.1016/j.apenergy.2019.05.069>
- [11] M. T. Dunstan, F. Donat, A. H. Bork, C. P. Grey, and C. R. Müller, "CO<sub>2</sub> capture at medium to high temperature using solid oxide-based sorbents: Fundamental aspects, mechanistic insights, and recent advances," *Chem. Rev.*, vol. 121, no. 20, pp. 12681–12745, Oct. 2021. <https://doi.org/10.1021/acs.chemrev.1c00100>
- [12] V. Gaur, R. Asthana, and N. Verma, "Removal of SO<sub>2</sub> by activated carbon fibers in the presence of O<sub>2</sub> and H<sub>2</sub>O," *Carbon*, vol. 44, no. 1, pp. 46–60, Jan. 2006. <https://doi.org/10.1016/j.carbon.2005.07.012>
- [13] C. Qin, D. He, Z. Zhang, L. Tan, and J. Ran, "The consecutive calcination/sulfation in calcium looping for CO<sub>2</sub> capture: Particle modeling and behaviour investigation," *Chem. Eng. J.*, vol. 334, pp. 2238–2249, Feb. 2018. <https://doi.org/10.1016/j.cej.2017.11.169>
- [14] Z. Zhao, K. Patchigolla, Y. Wu, J. Oakey, E. J. Anthony, and H. Chen, "Performance study on Ca-based sorbents for sequential CO<sub>2</sub> and SO<sub>2</sub> capture in a bubbling fluidised bed," *Fuel Process. Technol.*, vol. 221, art. 106938, Oct. 2021. <https://doi.org/10.1016/j.fuproc.2021.106938>
- [15] N. Schewe, F. Maleki, G. Di Liberto, A. Gerdes, H. Idriss, G. Pacchioni, and C. Wöll, "Identification of intermediates in the reaction pathway of SO<sub>2</sub> on the CaO surface: From physisorption to sulfite to sulfate," *Chem. Eur. J.*,

- vol. 29, no. 23, art. e202203956, Apr. 2023. <https://doi.org/10.1002/chem.202203956>
- [16] L. Chen, C. Wang, T. Si, and E. J. Anthony, "Modelling the simultaneous calcination/sulfation behavior of limestone under circulating fluidized bed combustion conditions," *Fuel*, vol. 257, art. 116072, Dec. 2019. <https://doi.org/10.1016/j.fuel.2019.116072>
- [17] F. Wesenauer, C. Jordan, M. Pichler, A. Frei, M. Azam, S. Setoodeh Jahromy, M. Harasek, and F. Winter, "An unreacted shrinking core model serves for predicting combustion rates of organic additives in clay bricks," *Energy Fuels*, vol. 34, no. 12, pp. 16679–16692, Dec. 2020. <https://doi.org/10.1021/acs.energyfuels.0c03075>
- [18] J. Blamey, M. Zhao, V. Manovic, E. J. Anthony, D. R. Dugwell, and P. S. Fennell, "A shrinking core model for steam hydration of CaO-based sorbents cycled for CO<sub>2</sub> capture," *Chem. Eng. J.*, vol. 291, pp. 298–305, May 2016. <https://doi.org/10.1016/j.cej.2016.01.086>
- [19] A. Amiri, G. Ingram, N. Maynard, I. Livk, and A. Bekker, "An unreacted shrinking core model for calcination and similar solid-to-gas reactions," *Chem. Eng. Commun.*, vol. 202, no. 9, pp. 1161–1175, Sep. 2015. <https://doi.org/10.1080/00986445.2014.910771>
- [20] J. M. Cordero and M. Alonso, "Modelling of the kinetics of sulphation of CaO particles under CaL reactor conditions," *Fuel*, vol. 150, pp. 501–511, Jun. 2015. <https://doi.org/10.1016/j.fuel.2015.02.075>
- [21] S.-M. Shih, J.-C. Lai, and C.-H. Yang, "Kinetics of the reaction of dense CaO particles with SO<sub>2</sub>," *Ind. Eng. Chem. Res.*, vol. 50, no. 22, pp. 12409–12420, Nov. 2011. <https://doi.org/10.1021/ie2009668>
- [22] L. Chen, C. Wang, F. Zhao, C. Zou, and E. J. Anthony, "The combined effect of H<sub>2</sub>O and SO<sub>2</sub> on the simultaneous calcination/sulfation reaction in CFBs," *AIChE J.*, vol. 65, no. 4, pp. 1256–1268, Apr. 2019. <https://doi.org/10.1002/aic.16531>
- [23] G. Vola, L. Sarandrea, G. Della Porta, A. Cavallo, F. Jaddoul, and G. Cruciani, "The influence of petrography, mineralogy and chemistry on burnability and reactivity of quicklime produced in Twin Shaft Regenerative (TSR) kilns from Neoproterozoic limestone (Transvaal Supergroup, South Africa)," *Mineral. Petrol.*, vol. 112, no. 4, pp. 555–576, Aug. 2018. <https://doi.org/10.1007/s00710-017-0542-y>
- [24] D. Li, Y. Wang, and Z. Li, "Limestone calcination kinetics in microfluidized bed thermogravimetric analysis (MFB-TGA) for calcium looping," *Catalysts*, vol. 12, no. 12, art. 1661, Dec. 2022. <https://doi.org/10.3390/catal1212166>
- [25] Arcenegui-Troya, P. E. Sánchez-Jiménez, A. Perejón, and L. A. Pérez-Maqueda, "Relevance of particle size distribution to kinetic analysis: The case of thermal dehydroxylation of kaolinite," *Processes*, vol. 9, no. 10, art. 1852, Oct. 2021. <https://doi.org/10.3390/pr9101852>
- [26] M. Izadifar, P. Thissen, A. Steudel, R. Kleeberg, S. Kaufhold, J. Kaltenbach, R. Schuhmann, F. Dehn, and K. Emmerich, "Comprehensive examination of dehydroxylation of kaolinite, disordered kaolinite, and dickite: Experimental studies and density functional theory," *Clays Clay Miner.*, vol. 68, no. 4, pp. 319–333, Aug. 2020. <https://doi.org/10.1007/s42860-020-00082-w>
- [27] R. Zevenhoven, P. Yrjas, and M. Hupa, "Sulfur dioxide capture under PFBC conditions: The influence of sorbent particle structure," *Fuel*, vol. 77, no. 4, pp. 285–292, 1998. [https://doi.org/10.1016/S0016-2361\(97\)00205-6](https://doi.org/10.1016/S0016-2361(97)00205-6)
- [28] L. N. Kashapov, N. F. Kashapov, and V. Y. Chebakova, "Mathematical simulation of cathode processes during hydrogen production," *Theor. Found. Chem. Eng.*, vol. 58, no. 3, pp. 595–600, Jun. 2024. <https://doi.org/10.1134/S0040579524601031>
- [29] L. Zhou, T. Lei, D. Kang, Y. Guo, Y. Zhang, F. Yang, M. Ge, and W. Wang, "Kinetics of heterogeneous reaction of H<sub>2</sub>O<sub>2</sub> and SO<sub>2</sub> on coal fly ash: Temperature effect and their synergistic effects," *Front. Environ. Sci.*, vol. 10, art. 876289, Jun. 2022. <https://doi.org/10.3389/fenvs.2022.876289>
- [30] P. Yuan, M. Li, S. Chen, and W. Xiang, "Thermodynamic properties and reaction mechanism of coal reductive decomposition phosphogypsum to prepare CaO and SO<sub>2</sub>," *Chin. J. Chem. Eng.*, vol. 79, pp. 135–144, Mar. 2025. <https://doi.org/10.1016/j.cjche.2024.11.011>
- [31] D. S. Ferreira, L. C. L. d. Santos, S. S. Santana, G. Simonelli, and K. R. d. O. Pereira, "Predictive modeling of demulsification efficiency in Brazilian crude oil: A statistical investigation of operational conditions," *Rev. Gestão Secretariado*, vol. 16, no. 5, art. e4878, Jan. 2025. <https://doi.org/10.7769/gesec.v16i5.4878>
- [32] M. Eriksson, K. Sandström, M. Carlborg, and M. Broström, "Impact of limestone surface impurities on quicklime product quality," *Minerals*, vol. 14, no. 3, art. 244, Feb. 2024. <https://doi.org/10.3390/min14030244>
- [33] P. Kong, J. Sun, K. Li, L. Jiang, R. Sun, T. Zhang, and Z. Zhou, "Insight into the deactivation mechanism of CaO-based CO<sub>2</sub> sorbent under in-situ coal combustion," *Sep. Purif. Technol.*, vol. 346, art. 127529, Oct. 2024. <https://doi.org/10.1016/j.seppur.2024.127529>
- [34] W. L. Li, X. Y. Gao, Y. Ouyang, J. Q. Wang, G. W. Chu, H. K. Zou, Y. Xiang, and J. F. Chen, "CFD analysis of gas flow characteristics and residence time distribution in a rotating spherical packing bed," *Ind. Eng. Chem. Res.*, vol. 58, no. 47, pp. 21717–21729, Nov. 2019. <https://doi.org/10.1021/acs.iecr.9b03625>
- [35] H. K. Hassan, S. A. Nosier, I. Hassan, M. H. Abdel-Aziz, G. H. Sedahmed, and M. A. El-Naggar, "Mass transfer behaviour and energy utilization efficiency of gas sparged rotating cylinder reactor and possible applications," *Chem. Eng. Process. - Process Intensif.*, vol. 178, art. 109043, Aug. 2022. <https://doi.org/10.1016/j.cep.2022.109043>
- [36] M. S. Parandin, H. Ale Ebrahim, and H. R. Norouzi, "Towards random pore model for non-catalytic gas-solid reactions," *Renew. Sustain. Energy Rev.*, vol. 202, art. 114731, Sep. 2024. <https://doi.org/10.1016/j.rser.2024.114731>
- [37] Y. Li, H. Tong, Y. Zhuo, C. Chen, and X. Xu, "Simultaneous removal of SO<sub>2</sub> and trace SeO<sub>2</sub> from flue gas: Effect of product layer on mass transfer," *Environ. Sci. Technol.*, vol. 40, no. 13, pp. 4306–4311, Jul. 2006. <https://doi.org/10.1021/es052381s>

- [38] I. Omidi Bibalani and H. Ale Ebrahim, "Comparison of sulfur dioxide removal reactions kinetics by  $\text{Na}_2\text{CO}_3$  and other different sorbents from coal-fired power plants," *Chem. Biochem. Eng. Q.*, vol. 36, no. 3, pp. 195–205, Dec. 2022. <https://doi.org/10.15255/CABEQ.2022.2069>
- [39] H. Moshiri, B. Nasernejad, H. A. Ebrahim, and M. Taheri, "A comprehensive kinetic study of the reaction of  $\text{SO}_2$  with  $\text{CaO}$  by the random pore model," *Chem. Eng. Technol.*, vol. 37, no. 12, pp. 2037–2046, Dec. 2014. <https://doi.org/10.1002/ceat.201400285>